VOL. 16, NO. 3, 2017, 6-10
www.fke.utm.my/elektrika
ISSN 0128-4428

ELEKTRIKA
Journal of Electrical Engineering

Investigation of Michelson Interferometer Fiber Temperature Sensor Based on Single Mode-Multimode-Single Mode Fiber Structure

Ying Xuan Ng[1], **Asrul Izam Azmi**[2*], **Muhammad Yusof Mohd Noor**[2], **Ahmad Sharmi Abdullah**[2] and **Raja Kamarulzaman Raja Ibrahim**[1]

[1]Faculty of Science, Universiti Teknologi Malaysia, 81310 UTM Skudai, Johor, Malaysia.
[2]Faculty of Electrical Engineering, Universiti Teknologi Malaysia, 81310 UTM Skudai, Johor, Malaysia.

[*]Corresponding author: asrul@utm.my, Tel: 607-5557126

Abstract: A simple fiber temperature sensor based on Michelson interferometer is investigated experimentally. The sensor is formed successive splicing of a single mode fiber (SMF) spliced to a short section of multimode fiber (MMF) followed by another SMF, which also known as single mode-multimode-single mode (SMS) structure. Temperature response of three different sensor lengths of 10 mm, 20 mm and 30 mm are experimented with increasing and decreasing temperature. The sensor exhibits good linearity, stability and repeatability for the test range from room temperature to 180 °C. The highest sensitivity is attained by the 10 mm sensor with response ~0.108 nm/°C. Factors that affect sensitivity are discussed and related issues are addressed. This sensor is most suitable for low to intermediate temperature applications.

Keywords: Michelson interferometer, optical fiber sensor, sensor tip, SMS structure, temperature sensing.

1. INTRODUCTION

Optical fiber based sensors have been studied comprehensively over the last decades due to their many intrinsic advantages such as their small size, light weight, immunity to electromagnetic interference, remote operation and the possibility of multiplexing several sensors into the same optical fiber. It has been applied in many areas including structural monitoring and biomedical applications. Optical fiber sensing can be implemented by several configurations, including the in-fiber grating [1, 2], tapered fiber [3], multimode interference (MMI) fiber [4-6], and fiber interferometer [7-16].

In recent years, there are increasing numbers of fiber interferometer based temperature sensors have been proposed due to their simple structure and flexible approach. Fiber interferometer configuration can be divided into number of configurations including Fabry-Perot interferometer (FPI) [7], Mach-Zehnder interferometer (MZI) [8, 9] and Michelson interferometer (MI) [10-16]. MZI operates in transmission mode, while MI and FPI operate in reflection mode. Interferometer in transmission mode required a complicated sensor head setup where they must be in stagnate straight condition. Any micro or macro bending due to a little movement of the head sensor could contribute to the error reading of the sensor. On the other hand, interferometer in reflection mode is easy to setup, as it does not need any alignment to make the fiber in straight position. In fact, MI is actually a folded MZI but with the advantage of double path length effect which keeps the sensor head more compact and robust.

Number of research works related to fiber MI sensor has been reported recently. A MI form with a short length of Germania core optical fiber (Ge-fiber) spliced with standard single mode fiber (SMF) demonstrated to produce a large measurement range due to higher differential refractive index of the Ge-fiber compared with a conventional SMF [10]. However, the Ge-fiber is not a standard commercialized fiber, which increases the total cost for each sensor. In a recent work, a compact MI sensor based on partial angled polished at tip SMF is proposed for high temperature measurement [11] with the sensitivity of ~13 pm/°C. With partially angled polish tip, the incoming light is split into two beams producing a MI mechanism within an optical fiber. A different MI scheme, a core offset thin core fiber with SMF is demonstrated for simultaneous refractive index and temperature sensing with low cross sensitivity [12]. A MI sensor based on SMF and small-core dispersion compensation fiber is reported for high temperature measurement [13]. The sensor achieved sensitivity is up to 68.6 pm/°C owing to the large mode index difference of the dominant interference modes. By utilizing optical liquid in photonic crystal fiber with high thermo-optic coefficient, sensitivity can be enhanced by more than 2 orders than the typical all-glass MI temperature sensor [14]. However, the liquid filled sensor requires complex fabrication process and operation may be limited by low temperature range and not suitable to be deployed in harsh environment.

This paper investigates the response of MI sensor based on SMF and multimode fiber (MMF) in SMF-MMF-SMF (SMS) configuration. Previously, there are few research works have reported the same sensor configuration with sensor tip is coated with highly reflective material to improve signal to noise ratio (SNR) of the reflected light [15, 16]. Distinguished from the previously reported works, this paper investigates the effects of length to performance of the temperature sensor. Furthermore, the SMS based MI configuration is constructed from standard SMF and MMF which reduces overall fabrication complexity and cost

2. THEORY

Fiber temperature sensor used in the experiment is constructed by successive connection of SMS which forms a MI as shown in Figure 1. The SMS scheme is totally different from the standard SMS structure [4, 5] that uses MMF as the sensing fiber based on the MMI effect. In the current work of the SMS configuration, the MMF functioned as a mode coupler to excite both core mode and cladding modes in the sensing SMF, while the second SMF acted as a sensing element. The length of the MMF must be kept shorter than a certain length to avoid MMI effect in the MMF. By doing that, this SMS structure can easily excite enough core and cladding modes to form a good maximum fringe visibility of interference spectrum which affect the SNR of the sensor. Both parts of light will be reflected at the cleaved ends of the SMF2 due to the Fresnel reflection and then recombined into MMF and SMF1, resulting in Michelson interference. The sensor is sensitive to surrounding temperature variation, due to the different thermo-optic coefficients of the fiber core and cladding in the SMS structure. This means that the core mode and cladding modes in the SMF2 change differently with temperature variation. It contributes to the phase shift, resulting wavelength shift of the dip or peak in the reflection spectra.

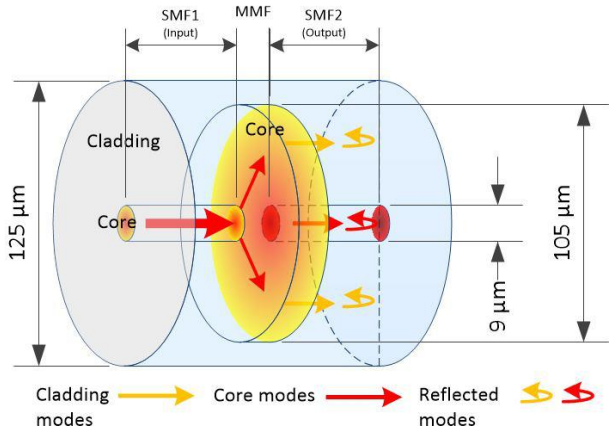

Figure 1. Schematic of MI fiber sensor

The reflectance of the MI structure can be represented in terms of interference between the core mode and m^{th} cladding mode which is given by a well-known interference equation [17]:

$$I = I_{core} + \sum_m I_{clad}^m + \sum_m 2\sqrt{I_{core} I_{clad}^m} \cdot \cos\Phi^m , \quad (1)$$

where I_{core} and I_{clad}^m are the intensity in the core mode and the m^{th} cladding mode, Φ^m is the phase difference between the core and m^{th} cladding modes which can be written as:

$$\Phi^m = \frac{2\pi \Delta n_{eff}^m L}{\lambda} , \quad (2)$$

where Δn_{eff}^m is the difference of the effective refractive index between the core and the m^{th} cladding modes; L is the round-trip length of SMF2; and, λ is the signal wavelength. The dips of interference spectrum occur when $\Phi = (2N+1)\pi$, where N is a positive integer. Hence, wavelength of the dip can be obtained as follows:

$$\lambda_N = \frac{2\Delta n_{eff}^m L}{2N+1} . \quad (3)$$

The free spectral range (FSR) or wavelength spacing between two successive interference dips, $\Delta\lambda$ can be written by:

$$\Delta\lambda = \frac{\lambda^2}{\Delta n_{eff}^m L} . \quad (4)$$

It is apparent that, with increased of the length, the FSR will be decreased. On the other hand, the dip wavelength shift, caused by temperature variations (or temperature sensitivity) is obtainable by differentiating equation (3) with respect to temperature. The resulting equation can be written as:

$$\Delta\lambda_N = \left[\frac{1}{\Delta n_{eff}^m} \frac{d(\Delta n_{eff}^m)}{dT} + \frac{1}{L}\frac{dL}{dT} \right] \Delta T \cdot \lambda_N \quad (5)$$

where dn/dT is the thermo-optic coefficient (8.6×10^{-6} K^{-1}) and $1/L(dL/dT)$ is the thermal-expansion coefficient of silica fiber (0.55×10^{-6} K^{-1}). Both effects contribute to the change to the wavelength shift of the sensor, with the effect of thermo-optic is more dominant.

Based on the structure, a numerical simulation is carried out using BeamPROP™ software in order to examine the field distribution internally. Only half of the propagation is simulated due to the limitation of the software to deal with reflection surface. As shown in Figure 2(a), as light reached the MMF, it is split into core and cladding modes. A portion of the core and cladding modes is assumed to be reflected at the flat tip of the fiber due to the index difference between glass and air. Figure 2(a) and (b) show the field distribution and the corresponding power along (0, 0, z) path at 30 °C. Parameters for the simulation are set as the following: the core effective refractive index is set 1.452; cladding refractive index is 1.4468; SMF1 and SMF3 length is 10 mm; and, MMF length is 0.3 mm. The light source is a 1553 nm Gaussian beam with unity amplitude.

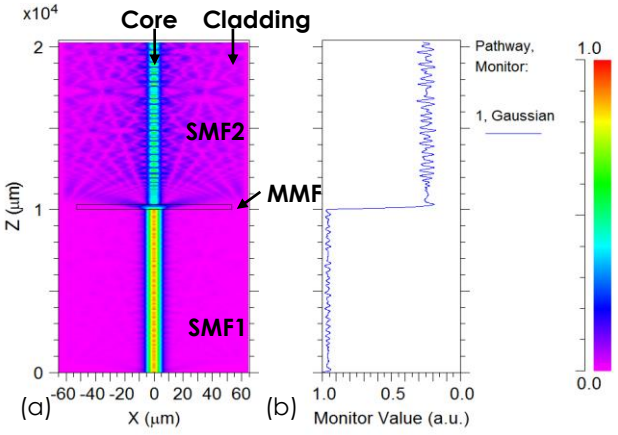

Figure 2. (a) Field distribution of the MI sensor, and (b) Trace of optical power along (0, 0, *z*) path

3. METHODOLOGY

Sample preparation process only requires cleaving and splicing which can be done using in-house facilities. Cleaving process in particular requires accuracy, thus this process is assisted by a microscope. The SMF and MMF have core/cladding diameters of 9 μm/125 μm and 105 μm/125 μm, respectively. Three different sensor (SMF2) length are prepared and tested; 10 mm, 20 mm and 30 mm, while MMF length is kept at ~0.3 mm for all samples. Initially, 30 mm sensor is prepared. Thus, the sensor part is repeatedly cleaved in order to obtain the other desired lengths (i.e. 20 mm and 10 mm). Splicing is done using Fujikura FSM-60S Fusion Splicer machine set with automatic splicing mode.

The experimental setup to examine the response of the sensor is shown in Figure 3. The system consists of a C-band amplified spontaneous emission source (model Photonic P-ASE-C-20-NF-F/A), a circulator, a dry heat oven (Venticell), an optical spectrum analyzer (OSA; model ANDO AQ6317B), and a computer which connect to the OSA using a National Instrument GPIB-USB-HS+ cable. The light source emits light which passed through the circulator and reach the sensor. Then, the sensor reflects the light and it will be received by the OSA. Sensor spectra are continuously recorded at the desired temperature interval.

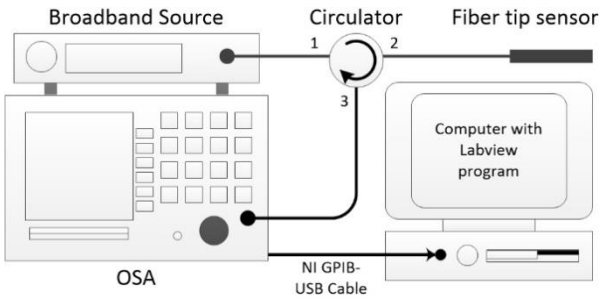

Figure 3. Experimental setup to test temperature response of the sensor

4.0 RESULTS AND DISCUSSION

Reflection spectra of all the samples are firstly compared to observe the difference of different sensor length. All samples exhibit different fringe contrast and wavelength spacing between adjacent interference dips which can be seen from the reflection spectra shown in Figure 4. The wavelength spacing is inversely proportional to the SMF2 length, where shorter sensor is expected to have larger dip spacing. The result shown in Figure 4 is in a good agreement with the equation (3), where the shortest SMF2 length (10 mm) exhibits the largest wavelength spacing compared to the other two lengths.

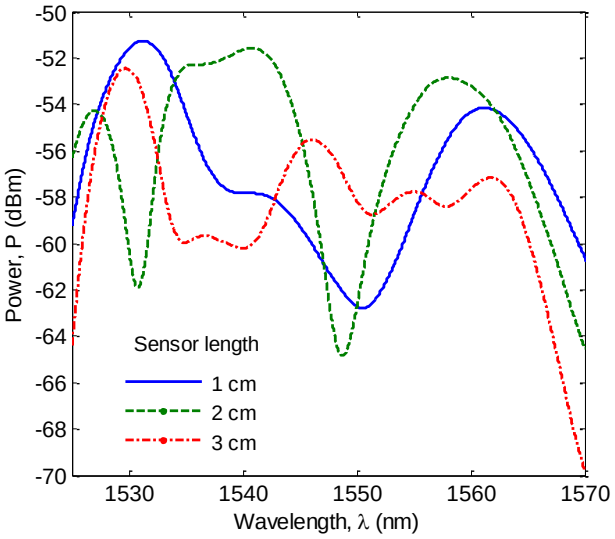

Figure 4. Reflection spectra of MI sensors with different sensor (SMF2) length at 30 °C

All sensors are experimented over the same temperature range from room temperature to 180 °C. Sensors are tested with increasing and decreasing temperature and the results are shown in Figure 5, 6, and 7. For 10 mm sensor, the highest contrast of fringe visibility is found from dip #2 at 1550.2 nm as can be seen in inset of Figure 5. Another dip (#1) can be found at 1540 nm, with very good linearity but lower sensitivity of ~-0.014 nm/°C for the increased and decreased temperature. On the other hand for dip #2, there is a slight discrepancy of the measured data from the linear fit when temperature is increased from 70 °C to 120 °C. Nonetheless, the R-squared of this measured points is larger than 0.967, suggesting a good linearity. The sensitivities shown for this dip is much higher at 0.109 nm/°C and 0.106 nm/°C for increasing and decreasing temperature, respectively. It can be seen, as the temperature is gradually increased towards 180 °C, dip #1 becoming more apparent while dip #2 gradually suppressed.

The temperature response for the 20 mm sensor is shown in Figure 6. There are two highly visible dips can be observed at 1530.7 nm (dip #1) and 1550 nm (dip #2). The measured sensitivities for dip #1 and dip #2 are ~0.074 nm/°C and ~0.085 nm/°C, which lower than that of 10 mm sensor. This sensor also exhibits better linearity than the previous sensor from the obtained R-squared value which higher than 0.99. For dip #2, the operational range only up to 130 °C before it is disappeared. Meanwhile, for the 30 mm sensor, there are more peaks and dips in the reflection spectra which can be used to obtain the temperature response. As can be seen in Figure 7, three distinguishable points are selected for the 30 mm sensor i.e. dip #1 (0.052 nm/°C), peak #1 (0.063 nm/°C) and dip #2 (0.080 nm/°C,

not shown). It can be noticed that the highest sensitivity of the 30 mm sensor is lower than that of the 10 mm and 20 mm sensors. Meanwhile, the obtained R-squared of this sensor is higher than 0.98 which can be considered as good in term of linearity.

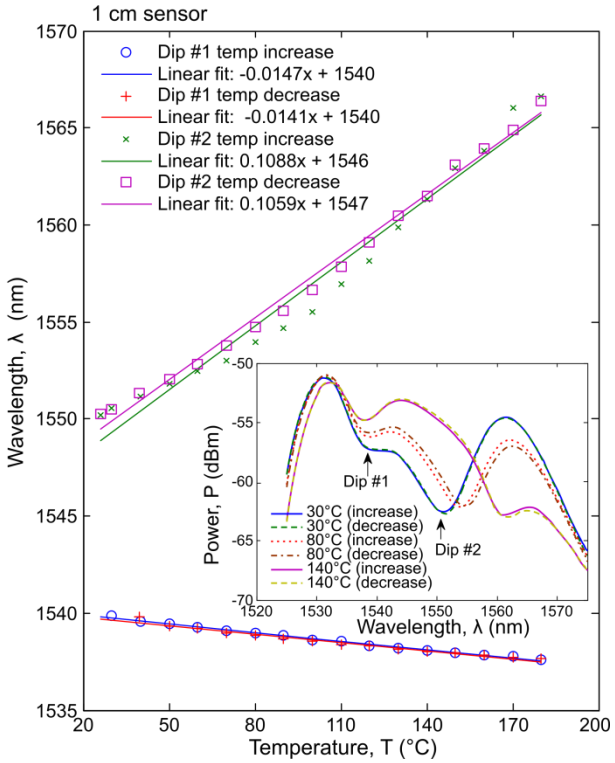

Figure 5. Measured dip wavelength of 10 mm sensor for increasing and decreasing temperature (inset shows reflection spectra at three different temperatures)

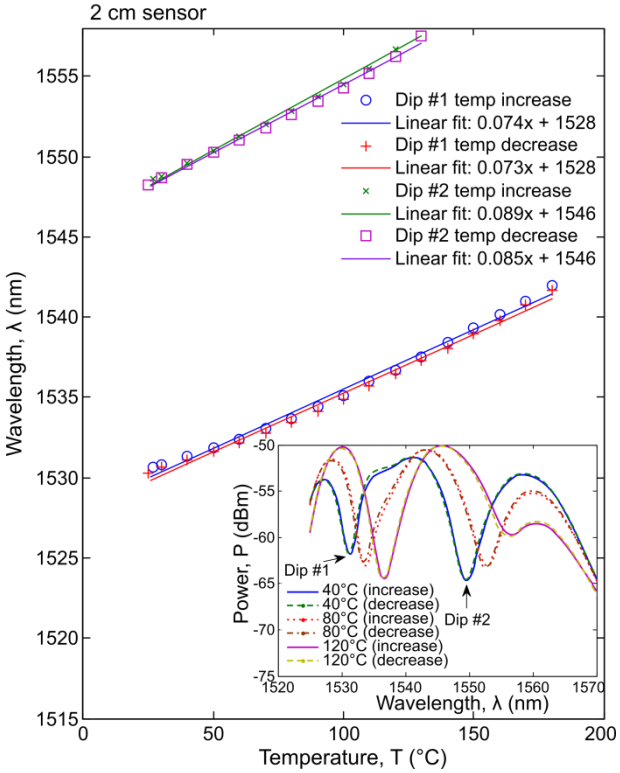

Figure 6. Measured dip wavelength of 20 mm sensor for increasing and decreasing temperature (inset shows reflection spectra at three different temperatures)

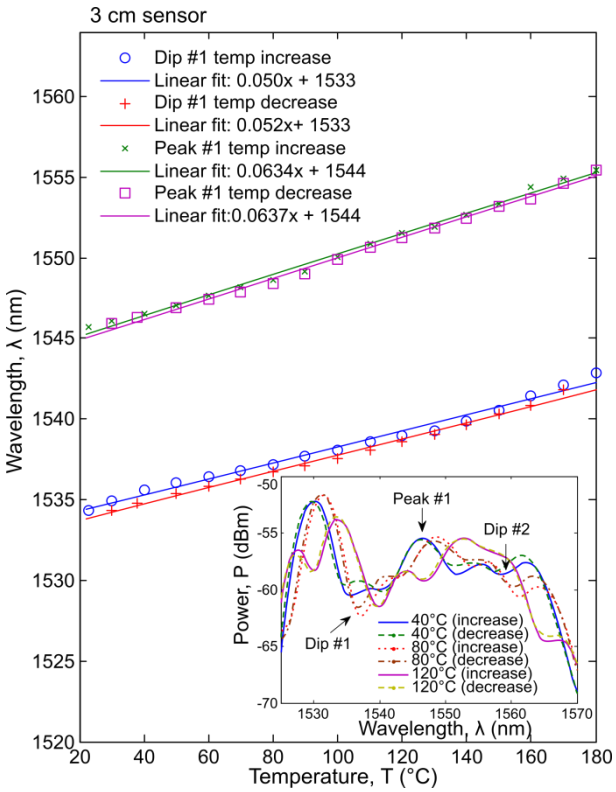

Figure 7. Measured dip wavelength and peak wavelength of 30 mm sensor for increasing and decreasing temperature (inset shows reflection spectra at three different temperatures)

It can be observed that the amount of shift is dependent on the initial dip/peak wavelength. For all sensors the dips at higher wavelength shift more rapidly compared with the dips at lower wavelength which well agreed according to equation (5). It is noticed that the sensor length affects the sensitivity to a certain extent, where the highest sensitivity is exhibited by 10 mm sensor, followed by 20 mm sensor. Evidently, increasing the length may not necessarily will increase the temperature sensitivity as there are other factors such as number of modes excited into cladding which may require further investigation.

Response of dip #1 for both 10 mm and 20 mm sensors are desired, as these dips provide linear and stable response over the measured range. While the dips at higher wavelength (i.e. dip #2 for both 10 mm and 20 mm sensors), exhibit higher sensitivity, but could not sustain linear response over the required temperature range. Both 20 mm and 30 mm sensors demonstrate consistent response for increasing and decreasing temperature. The dip wavelength for decreased temperature seems to follow slightly different path of shifting compared with the increased temperature, expected from the thermal induced residual stress that has not been fully released inside the fiber during the cooling period.

5.0 CONCLUSION

We have investigated a very simple, low cost and wide range fiber Michelson interferometer based temperature sensor with different sensor lengths. Factors that affect sensitivity are discussed and related issues are addressed. This fiber tip temperature sensor able to respond well in temperature ranged from room temperature to 180 °C, with

the highest sensitivity of 0.108 nm/°C for 10 mm sensor length. This sensor exhibits repeatable spectra for a specific temperature as it is tested with rise and fall of temperature. Moreover, the proposed fiber tip temperature sensor has the advantages which are compact size, have good stability, response, and high dynamic range. Therefore, the performance of this sensor possesses a great potential in many fields that require low to intermediate temperature sensing capability.

ACKNOWLEDGMENT

We wish to acknowledge for the support received from the Research University Grant, 12J50 by Ministry of Higher Education, Malaysia.

REFERENCES

[1] T. Liu, Y. Chen, Q. Han, F. Liu and Y. Yao, "Sensor based on macrobent fiber Bragg grating structure for simultaneous measurement of refractive index and temperature," *Appl. Optics*, vol. 55, pp. 791-795, February 2016.

[2] Q. Wu and Y. Okabe, "High-sensitivity ultrasonic phase-shifted fiber Bragg grating balanced sensing system," *Optics Express*, vol. 20, pp. 28353-28362, December 2012.

[3] Y. Tian, W. Wang, N. Wu, X. Zou and X. Wang, "Tapered optical fiber sensor for label-free detection of biomolecules," *Sensors*, vol. 11, pp. 3780-3790, March 2011.

[4] D. Song, Q. Chai, Y. Liu, Y. Jiang, J. Zhang, W. Sun, L. Yuan, J. Canning and G. Peng, "A simultaneous strain and temperature sensing module based on FBG-in-SMS," *Measurement Science and Technology*, vol. 25, pp. 055205, March 2014.

[5] M. Y. Mohd Noor, A. I. Azmi, A. S. Abdullah, A. S. Mohd Supa'at, N. Mohd Kassim, M. H. Ibrahim and N. H. Ngajikin, "High sensitivity of balloon-like bent MMI fiber low-temperature sensor," *IEEE Photonics Technology Letters*, vol. 27, pp. 1989-1992, June 2015.

[6] N. Bhatia and J. John, "Multimode interference devices with single-mode-multimode-multimode fiber structure," *Applied Optics*, vol. 53, pp. 5179-5186, August 2014.

[7] S. Wu, G. Yan, Z. Lian, X. Chen, B. Zhou and S. He, "An open-cavity Fabry-Perot interferometer with PVA coating for simultaneous measurement of relative humidity and temperature," *Sensors and Actuators B: Chemical*, vol. 225, pp. 50-56, March 2016.

[8] Q. Wu, Y. Okabe and J. Wo, "Fiber sensor based on interferometer and Bragg grating for multiparameter detection," *IEEE Photonics Technology Letters*, vol. 27, pp. 1345-1348, April 2015

[9] M. Shao, X. Qiao, H. Fu, H. Li, Z. Jia and H. Zhou, "Refractive index sensing of SMS fiber structure based Mach-Zehnder interferometer," *IEEE Photonics Technology Letters*, vol. 26, pp. 437-439, January 2014.

[10] J. Yang, Y. Zheng, L. H. Chen, C. C. Chan, X. Dong, P. P. Shum and H. Su, "Miniature temperature sensor with germania-core optical fiber," Optics Express, vol. 23, pp. 17687-17692, July 2015.

[11] J. Yin, T. Liu, J. Jiang, K. Liu, S. Wang, S. Zou and F. Wu, "Assembly-free-based fiber-optic micro-Michelson interferometer for high temperature sensing," *IEEE Photonics Technology Letters*, vol. 28, pp. 625-628, November 2015.

[12] J. Zhou, Y. Wang, C. Liao, B. Sun, J. He, G. Yin, S. Liu, Z. Li, G. Wang, X. Zhong and J. Zhao, "Intensity modulated refractive index sensor based on optical fiber Michelson interferometer," Sensors and Actuators B: Chemical, vol. 208, pp. 315-319, March 2015.

[13] B. Dong, L. Wei and D. "Miniature high-sensitivity high-temperature fiber sensor with a dispersion compensation fiber-based interferometer," *Applied Optics*, vol. 48, pp. 6466-6469, November 2009.

[14] J. Hsu, J. Horng, C. Hsu and C. Lee, "Fiber-optic Michelson interferometer with high sensitivity based on a liquid-filled photonic crystal fiber," Optics Communications, vol. 331, pp. 348-352, November 2014.

[15] Q. Rong, X. Qiao, Y. Du, D. Feng, R. Wang, Y. Ma, H. Sun. M. Hu and Z. Feng, "In-fiber quasi-Michelson interferometer with a core-cladding-mode fiber end-face mirror," *Applied Optics*, vol.52, pp. 1441-1447, March 2013.

[16] Y. Zhang, A. Zhou, B. Qin, H. Deng, Z. Liu, J. Yang and L. Yuan, "Refractive index sensing characteristics of single-mode fiber-based modal interferometers," *J. of Lightwave Technology*, vol. 32, pp. 1734-1740, May 2014.

[17] D. Wu, K. S. Chiang and M. Deng, "All Single-Mode Fiber Mach–Zehnder Interferometer Based on Two Peanut-Shape Structures," *J. of Lightwave Technology*, vol. 30, pp. 805-810, March 2012.